

Targeted vertical cross-sectional imaging with handheld near-infrared dual axes confocal fluorescence endomicroscope

Zhen Qiu,¹ Zhongyao Liu,² Xiyu Duan,¹ Supang Khondee,² Bishnu Joshi,²
Michael J. Mandella,⁵ Kenn Oldham,³ Katsuo Kurabayashi,^{3,4} and
Thomas D. Wang^{1,2,3,*}

¹Department of Biomedical Engineering, University of Michigan, Ann Arbor, MI 48109, USA

²Department of Medicine, Division of Gastroenterology, University of Michigan, Ann Arbor, MI 48109, USA

³Department of Mechanical Engineering, University of Michigan, Ann Arbor, MI 48109, USA

⁴Department of Electrical Engineering and Computer Science, University of Michigan, Ann Arbor, MI 48109, USA

⁵Department of Pediatrics, Stanford University School of Medicine, Stanford, CA 94305, USA

*thomaswa@umich.edu

Abstract: We demonstrate vertical cross-sectional (XZ-plane) images of near-infrared (NIR) fluorescence with a handheld dual axes confocal endomicroscope that reveals specific binding of a Cy5.5-labeled peptide to pre-malignant colonic mucosa. This view is perpendicular to the tissue surface, and is similar to that used by pathologists. The scan head is 10 mm in outer diameter (OD), and integrates a one dimensional (1-D) microelectromechanical systems (MEMS) X-axis scanner and a bulky lead zirconate titanate (PZT) based Z-axis actuator. The microscope images in a raster-scanning pattern with a ± 6 degrees (mechanical) scan angle at ~ 3 kHz in the X-axis (fast) and up to 10 Hz (0–400 μm) in the Z-axis (slow). Vertical cross-sectional fluorescence images are collected with a transverse and axial resolution of 4 and 5 μm , respectively, over a field-of-view of 800 μm (width) \times 400 μm (depth). NIR vertical cross-sectional fluorescence images of fresh mouse colonic mucosa demonstrate histology-like imaging performance with this miniature instrument.

© 2013 Optical Society of America

OCIS codes: (170.1790) Confocal microscopy; (170.3880) Medical and biological imaging; (170.4580) Optical diagnostics for medicine; (170.5810) Scanning microscopy.

References and links

1. T. D. Wang, S. Friedland, P. Sahbaie, R. Soetikno, P. L. Hsiung, J. T. C. Liu, J. M. Crawford, and C. H. Contag, “Functional imaging of colonic mucosa with a fibered confocal microscope for real-time *in vivo* pathology,” *Clin. Gastroenterol. Hepatol.* **5**(11), 1300–1305 (2007).
2. R. Kiesslich, J. Burg, M. Vieth, J. Gnaediger, M. Enders, P. Delaney, A. Polglase, W. McLaren, D. Janell, S. Thomas, B. Nafe, P. R. Galle, and M. F. Neurath, “Confocal laser endoscopy for diagnosing intraepithelial neoplasias and colorectal cancer *in vivo*,” *Gastroenterology* **127**(3), 706–713 (2004).
3. H. J. Shin, M. C. Pierce, D. Lee, H. Ra, O. Solgaard, and R. Richards-Kortum, “Fiber-optic confocal microscope using a MEMS scanner and miniature objective lens,” *Opt. Express* **15**(15), 9113–9122 (2007).
4. C. L. Arrasmith, D. L. Dickensheets, and A. Mahadevan-Jansen, “MEMS-based handheld confocal microscope for *in-vivo* skin imaging,” *Opt. Express* **18**(4), 3805–3819 (2010).
5. J. K. Kim, W. M. Lee, P. Kim, M. Choi, K. Jung, S. Kim, and S. H. Yun, “Fabrication and operation of GRIN probes for *in vivo* fluorescence cellular imaging of internal organs in small animals,” *Nat. Protoc.* **7**(8), 1456–1469 (2012).
6. D. Huang, E. A. Swanson, C. P. Lin, J. S. Schuman, W. G. Stinson, W. Chang, M. R. Hee, T. Flotte, K. Gregory, C. A. Puliafito, and J. G. Fujimoto, “Optical coherence tomography,” *Science* **254**(5035), 1178–1181 (1991).
7. K. S. Lee, H. Zhao, S. F. Ibrahim, N. Meemon, L. Khoudoir, and J. P. Rolland, “Three-dimensional imaging of normal skin and nonmelanoma skin cancer with cellular resolution using Gabor domain optical coherence microscopy,” *J. Biomed. Opt.* **17**(12), 126006 (2012).
8. N. Callamaras and I. R. Parker, “Construction of a confocal microscope for real-time x-y and x-z imaging,” *Cell Calcium* **26**(6), 271–279 (1999).
9. W. Göbel, B. M. Kampa, and F. Helmchen, “Imaging cellular network dynamics in three dimensions using fast 3D laser scanning,” *Nat. Methods* **4**(1), 73–79 (2007).

10. H. Mansoor, H. Zeng, K. Chen, Y. Yu, J. Zhao, and M. Chiao, "Vertical optical sectioning using a magnetically driven confocal microscanner aimed for *in vivo* clinical imaging," *Opt. Express* **19**(25), 25161–25172 (2011).
11. K. K. Ghosh, L. D. Burns, E. D. Cocker, A. Nimmerjahn, Y. Ziv, A. E. Gamal, and M. J. Schnitzer, "Miniaturized integration of a fluorescence microscope," *Nat. Methods* **8**(10), 871–878 (2011).
12. T. D. Wang, M. J. Mandella, C. H. Contag, and G. S. Kino, "Dual-axis confocal microscope for high-resolution *in vivo* imaging," *Opt. Lett.* **28**(6), 414–416 (2003).
13. J. T. C. Liu, M. J. Mandella, J. M. Crawford, C. H. Contag, T. D. Wang, and G. S. Kino, "Efficient rejection of scattered light enables deep optical sectioning in turbid media with low-numerical-aperture optics in a dual-axis confocal architecture," *J. Biomed. Opt.* **13**(3), 034020 (2008).
14. W. Piyawattanametha, H. Ra, Z. Qiu, S. Friedland, J. T. C. Liu, K. Loewke, G. S. Kino, O. Solgaard, T. D. Wang, M. J. Mandella, and C. H. Contag, "In *vivo* near-infrared dual-axis confocal microendoscopy in the human lower gastrointestinal tract," *J. Biomed. Opt.* **17**(2), 021102 (2012).
15. L. K. Wong, M. J. Mandella, G. S. Kino, and T. D. Wang, "Improved rejection of multiply scattered photons in confocal microscopy using dual-axes architecture," *Opt. Lett.* **32**(12), 1674–1676 (2007).
16. P. L. Hsiung, J. Hardy, S. Friedland, R. Soetikno, C. B. Du, A. P. Wu, P. Sahbaie, J. M. Crawford, A. W. Lowe, C. H. Contag, and T. D. Wang, "Detection of colonic dysplasia *in vivo* using a targeted heptapeptide and confocal microendoscopy," *Nat. Med.* **14**(4), 454–458 (2008).
17. S. J. Miller, C. M. Lee, B. P. Joshi, A. Gaustad, E. J. Seibel, and T. D. Wang, "Targeted detection of murine colonic dysplasia *in vivo* with flexible multispectral scanning fiber endoscopy," *J. Biomed. Opt.* **17**(2), 021103 (2012).
18. K. L. Turner, S. A. Miller, P. G. Hartwell, N. C. MacDonald, S. H. Strogatz, and S. G. Adams, "Five parametric resonances in a micro-electro-mechanical system," *Nature* **396**(6707), 149–152 (1998).
19. H. Schenck, P. Dürr, D. Kunze, H. Lakner, and H. Kück, "A resonantly excited 2D-micro-scanning-mirror with large deflection," *Sens. Actuators A Phys.* **89**(1–2), 104–111 (2001).
20. Z. Qiu, J. Pulskamp, X. Lin, C. H. Rhee, T. D. Wang, R. Polcawich, and K. Oldham, "Large displacement vertical translational actuator based on piezoelectric thin films," *J. Micromech. Microeng.* **20**(7), 075016 (2010).

1. Introduction

By convention, most pathologists review histology cut perpendicular to the tissue surface or in the vertical cross-section (XZ-plane) in order to visualize the normal (or abnormal) tissue maturation pattern. The vertical cross-section provides a comprehensive view of the epithelium in the digestive tract which normally differentiates in the basilar to luminal direction. This orientation also can accurately register the location of important biological behavior relative to the tissue surface. Imaging in this orientation has not been fully explored in endomicroscopy because most instruments do not have sufficient dynamic range to collect images in the vertical cross-section [1–5]. Imaging in the XY-plane (parallel to the tissue surface) visualizes tissue that tends to have similar microarchitecture over the field-of-view (FOV). The epithelium of hollow organs, such as the colon, is the origin of many important types of cancer. Imaging microstructures from the tissue surface to about half a millimeter deep can reveal early signs of disease and progression. The vertical cross-section presents histology-like images for diagnosis and quantitative studies of early cancer development. Imaging in this orientation is standard for traditional ultrasound (B-scan), optical coherence tomography (OCT) and optical coherence microscopy (OCM) [6,7].

Imaging in the vertical cross-section on endomicroscopy faces many technical challenges. Microelectromechanical systems (MEMS) and micro-optics technologies enable the development of miniature endomicroscopes within space constraints of millimeter dimensions [3,4]. An axial scanning method has been demonstrated that translates a bulky or miniature objective lens [8–10] placed in direct contact with the tissue. However, this strategy can introduce significant image distortions [11] and disturb the biological sample during imaging [8]. The confocal endomicroscope jointly developed by Pentax and Optiscan [2] uses a thin nitinol based wire actuator for Z-axis scanning inside the instrument. Unfortunately, the scanning speed of this actuator is limited, and the instrument can only perform en-face (XY-plane) imaging with Z-stack. The accuracy of the Z-axis scan can be influenced significantly by the hysteresis in the actuator.

In conventional microscopy, high numerical aperture (NA) objective lenses are used to achieve sub-cellular resolution. This strategy cannot be used in endomicroscopy without incurring a tradeoff in either working distance or FOV. The dual axes architecture [12] uses two low NA objectives and separate illumination and collection beams that intersect to achieve subcellular resolution in both the transverse and axial dimensions. The dual axes

configuration was first demonstrated as a table-top system [13] and then scaled down in size to millimeter dimensions using fiber coupling and post-objective scanning to provide a long working distance with a large FOV [14]. Also, the dual axes design was shown to have superior rejection of out-of-focus and multiply scattered light using Monte-Carlo analysis [15]. Moreover, using diffraction theory to determine the drop-off in the axial response, this configuration was shown to achieve a significant improvement in dynamic range compared to that of a comparable single axis design [13]. This property of the dual axes design allows for imaging in the vertical cross-section.

The use of molecular probes is an important, emerging direction in diagnostic imaging that improves specificity for disease detection and reveals biological function. Dysplasia is a premalignant condition in the colon that increases risk for progression onto cancer. Peptides have demonstrated tremendous potential for *in vivo* use to detect colonic dysplasia [16,17]. This class of *in vivo* molecular probe can be labeled with near-infrared (NIR) dyes for visualizing the full depth of the epithelium in small animals. Here, we aim to demonstrate vertical cross-sectional fluorescence images with a compact XZ-plane scanner that consists of an electrostatic MEMS resonant X-axis scanning mirror and a bulky PZT based Z-axis actuator to visualize specific peptide binding to dysplasia in the mouse colon.

2. Methods

2.1. Vertical cross-sectional imaging optical circuit design

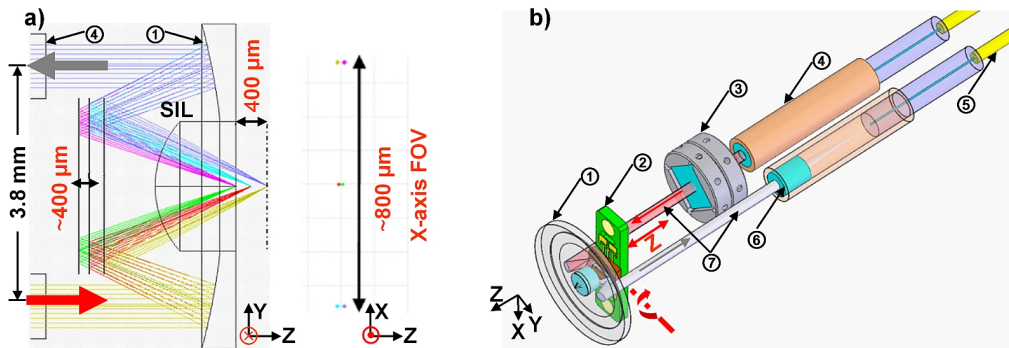


Fig. 1. Endomicroscope schematic. (a) Cross-sectional view of dual axes architecture shows ray-trace simulation in ZEMAX for achieving 800 μm (width) \times 400 μm (depth) images. (b) Optical circuit design for vertical cross-sectional imaging with fiber-coupled achromatic collimators. Components: (1) aluminum coated parabolic mirror with solid immersion lens (SIL) in center; (2) MEMS mirror with PCB holder; (3) prism with holder; (4) achromatic doublet lens based collimator; (5) single mode fiber; (6) achromatic lens; (7) illumination (red) and collection beam (gray).

We determined the scan parameters needed to achieve vertical cross-sectional images with the miniature dual axes design in colonic epithelium by performing ray-trace simulations in ZEMAX (Redmond, WA), Fig. 1(a). From these simulations, we found that we can achieve vertical cross-sectional images having an 800 μm (X-axis) FOV in the transverse dimension (X-axis) by requiring a MEMS scanner that has a mechanical scan angle of ± 6 degrees. The three pairs of spots represent the focus points of the illumination and collection beams at either extent of the scanning range and on axis. The relations from diffraction theory [13] give us a predicted lateral resolution of 1.9 μm on X-axis and 1.7 μm on Y-axis, and the predicted axial resolution is 4.2 μm (all at 671 nm wavelength). The Z-axis actuator moves the focal volume over a range of ~ 400 μm below the tissue surface, which is sufficient for imaging colonic epithelium in the mouse (< 200 μm) or human (< 500 μm). The scanning mirror in the optical circuit has the ability to be translated up to ~ 1 mm in a forward/backward direction by the z-axis actuator. However, the real vertical range for imaging is limited by beam-clipping at the outside diameter (1.8 mm) of the solid immersion lens (SIL, Fig. 1(a), no. 1).

Fluorescence excitation is provided by a solid-state diode laser (300 mW, CNI Laser Inc., Changchun, China) at $\lambda_{ex} = 671$ nm. The laser beam is coupled into a single mode fiber (S630-HP, NA = 0.12, Nufern, East Granby, CT). The illumination beam (0.95 mm $1/e^2$ diameter) is delivered by a custom-made fiber-coupled achromatic doublet lens (NT65-568, Edmund Optics, Barrington, NJ) collimator (2.99 mm focal length, GRINTECH GmbH, Jena, Germany). The optical path of the miniature dual axes microscope consists of two parallel and collimated beams, each being used to provide an illumination and a collection optical path, respectively as shown in Fig. 1(a). The collimators are fixed inside two parallel holes drilled using a computer numerical control (CNC) machine (Haas system). The illumination beam passes through two custom-made 0.1 deg optical wedges (Risley prisms) that are 3.5×3.5 mm² in dimension, made of N-BK7 glass, and anti-reflection coated with reflectivity <0.5% for 640-785 nm (Tower Optical, Boynton Beach, FL). Each Risley prism is held by a holder (Fig. 1(b), no. 3), which is located inside a sleeve through Class III medium fit. A miniature wrench is used to turn the processing holes. The Risley prisms provide fine adjustment to bring the illumination and collection beams into a parallel relationship within 0.05 degrees. Optimal alignment is then validated by measuring the lateral and axial resolution. The center-to-center distance between the collimated beams is 3.8 mm. The beams are deflected by a MEMS 1-D X-axis scanner, shown in Fig. 2, located in the post-objective position.

The mirror surface is coated with a 120 nm layer of gold (Au) on a 10 nm adhesion layer of chrome (Cr), providing a reflectivity of >85% for 640-785 nm for both illumination and collection. Axial scanning is performed with an XZ-plane scan engine which consists of an X-axis MEMS scanner and a Z-axis bulky PZT based actuator, shown in Fig. 3. The two collimated beams are then focused by an aluminum-coated parabolic mirror ($f = 4.6$ mm) through an index matching SIL (fused silica), and intersect below the tissue surface to define the focal volume. The SIL is inserted into the hole in the center of the parabolic mirror with a Class II free fit and sealed with UV-curable glue. The focusing half-angle of each beam and the intersection half-angle between the beams are 0.075 radians ($1/e^2$ intensity) and 24 deg, respectively, Fig. 1(a). This combination of achromatic collimators and reflective parabolic mirror results in a nearly achromatic focusing strategy. Light collected from the tissue sample is band-pass filtered ($T_{avg} > 93\%$ for 693-736 nm, FF01-716/40-25, Semrock, Rochester, NY) to block the unwanted excitation, and the remaining fluorescence is detected by a photomultiplier tube (PMT, H7422PA-40, Hamamatsu).

2.2. MEMS One-dimensional (1-D) X-axis resonant scanner

We have developed a 1-D MEMS resonant scanner (Fig. 2) for X-axis scanning using a working principle based on electro-static, parametric resonant tilting [18] to achieve a scan angle greater than the desired ± 6 degrees with a low drive voltage (<40 V) in a small 3×2 mm² footprint. The tilting mirror steers the two overlapping beams (illumination and collection) together over the FOV with a geometry that has a high fill-in factor of 90.3% (2.71 mm/3 mm) in the lateral dimension of the device (Fig. 2(a)). The tilting mirror requires an open area on the backside, which is realized with an advanced deep reactive-ion etching (DRIE, Deep Silicon Etcher, STS Pegasus 4", SPTS, San Jose, CA) process with high aspect ratio and steep side walls. With the in-plane vertical comb-drive configuration [19], MEMS resonant scanners require only a “3-step process” (Fig. 2(b)) using a 4-inch silicon-on-insulator (SOI) wafer (device silicon/buried oxide/handle silicon layer: 30/2/500, unit: μm), including: (1) patterned gold coating on the top side of device silicon for reflective mirror surface and electrical pads, (2) DRIE on the top silicon layer for vertical in-plane comb-drive actuators and mirror’s hinges, (3) DRIE on the bottom layer for an opening hole and buffered oxide etch (BOE) for releasing the tilting mirror.

During post-processing, each module (20×20 mm²) is diced (ADT 7100 Dicing Saw) from the SOI wafer with 5 μm photo-resist protection on the top side of the device silicon layer. Then, the protection photo-resist is removed by reactive-ion etching (RIE, LAM9400, LAM Research, Fremont, CA). Each device is dry-released from the module by breaking off the link-arm struts with laser cutting (or tweezers). With the simple robust fabrication and

fully dry post-process, the new application-driven MEMS scanner design and its fabrication process guarantee a high device yield (>90%). With parametric resonance, the mirror is driven by a square waveform (50% duty cycle) with drive frequency $f_{\text{drive}} = 2 \times f_{\text{res}}/N$ ($N = 1, 2, 3, \dots$, in ambient air, we use $N = 1$). The mirror surface is first coated with a 10 nm layer of Cr followed by a 120 nm layer of Au, for enhanced reflectivity (>85%, 640-785 nm) in the NIR. The MEMS devices are all developed in the Lurie Nanofabrication Facility (LNF) at the University of Michigan.

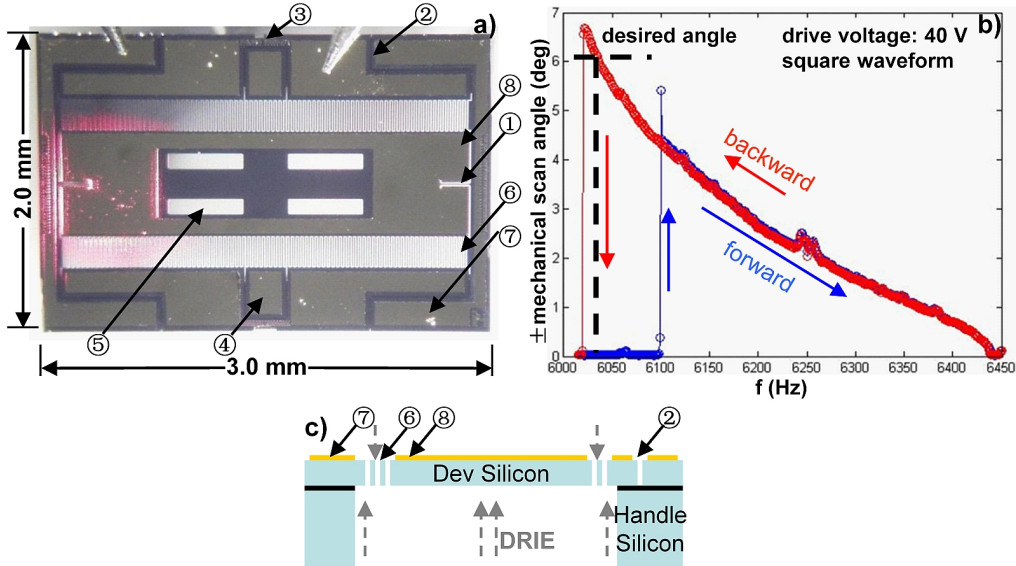


Fig. 2. MEMS 1-D (X-axis) resonant scanner. (a) Stereomicroscope image of mirror. Red spot represents reflected He-Ne (633nm) laser beam from gold coated reflective surface. Components: (1) hinge; (2) electric isolation trench; (3) link-arm struts; (4) sensor pad; (5) four weight-reducing holes; (6) electrostatic comb-drive actuators; (7) electric Au/Cr pad; (8) Au/Cr coated reflective mirror surface. (b) Frequency response of MEMS scanner is shown from sweeping the frequency with 10 Hz step size, forward (blue) and backward (red) with 40 V and 50% duty cycle. (c) Schematic of cross-sectional view of the MEMS 1-D scanner design for a $3 \times 2 \text{ mm}^2$ SOI device with pattern gold coating using DRIE on the top and bottom layers.

The response curve of the MEMS resonant scanner is shown in Fig. 2(c). The mirror is excited to start tilting and reaches the peak amplitude by sweeping the pulse width modulation (PWM, 0 to 50%, with 10% step size) of a square waveform in 1.0 sec initiation time by fixing the drive frequency at a desired value for imaging. For example, the resonant frequency of the tilting mirror is 3010 Hz at a drive frequency of 6020 Hz, $f_{\text{res}} = f_{\text{drive}} \times N/2$, $N = 1$. Meanwhile, synchronization of the phase between the driving waveform on X-axis and Z-axis, which is the key for vertical cross-sectional imaging at fast frame rates, is achieved using custom LabVIEW (National Instruments, Austin, TX) software.

2.3. XZ-plane scan engine design for vertical cross-sectional imaging

We developed a novel and compact optomechanical design for an axial scanning mechanism. For our application, we need to realize a raster-scanning pattern with kHz tilting speeds at 2-10 Hz frame rates over a Z-axis range of 0-400 μm , Fig. 3(a). To perform axial scanning with a fast pure z-axis fast motion, we have developed a handheld “proof-of-concept” design that provides us an opportunity to study the vertical cross-sectional imaging in a miniature dual axes endomicroscope. The instrument package, shown in Fig. 3, is realized fully in stainless steel (Protomatic, Dexter, MI) and is sealed by epoxy glue. An electro-static MEMS 1-D X-axis resonant scanner is located in the post-objective position, and is directly integrated onto the Z-axis actuator through a PCB and cantilever (Fig. 3(a)) that can be well aligned along the Z-axis and located closely to the parabolic mirror at the end. Using the “T-shape” mechanical

cantilever linker (Fig. 3, no. 2), the scanner and its PCB are all directly mounted onto the tip of the bulky PZT based Z-axis actuator with embedded strain gauge sensor (P601.4SL, Physik Instrumente, Auburn, MA) that translates the focal volume into the tissue over a range of 0–400 μm with 0 degree tilt angle (Fig. 3(b)). The MEMS mirror is secured onto the PCB with low stress silver epoxy, and while scanning in resonant mode (>3 kHz), this device is not affected by low frequency vibrations (<100 Hz) produced by the Z-axis actuator.

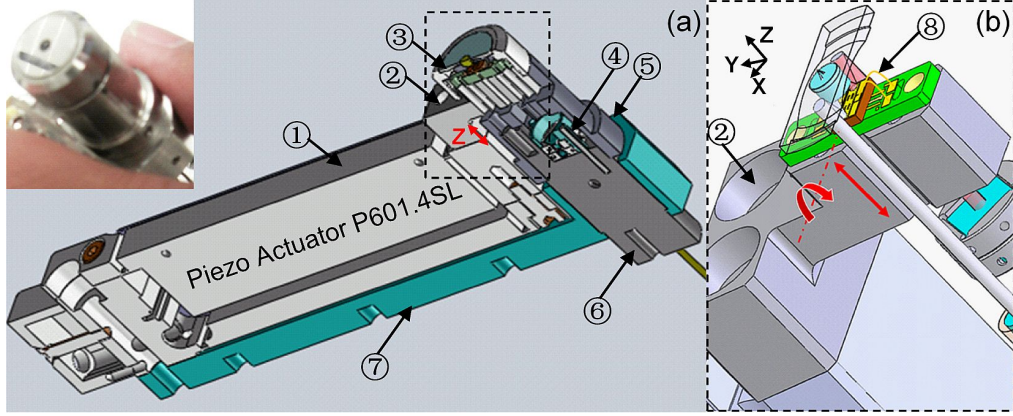


Fig. 3. Schematic of handheld dual axes endomicroscope packaging. (a) Cross-sectional view of system packaging without protection shell shows inner integrated XZ-plane 2D scan engine for vertical cross-sectional imaging (inset: handheld prototype); (b) Magnified view of XZ-plane 2D scan engine design. Components: (1) Z-axis piezo actuator; (2) “T-shape” cantilever on the tip of PZT actuator; (3) parabolic mirror and its holder; (4) prism holder clamp; (5) tube jacket; (6) collimator housing tube; (7) PZT actuator holder; (8) Au bonding wire for electricity connection.

2.4. Control, data acquisition and reconstruction

We used a multifunction data acquisition board (PCI-6115, National Instruments, Austin, TX) and 2-channel function generator (33522A, Agilent, Santa Clara, CA) to operate the instrument. The MEMS scanner and Z-axis actuator are driven with a square and an edge-smoothed triangle waveform, respectively, using a 2-channel high voltage amplifier (TEGAM 2350, Geneva, Ohio). The FOV and frame rate for the images collected are determined by the amplitude and frequency of these control signals. 2-D vertical cross-sectional fluorescence images are acquired and displayed in real time to enable continuous visualization. All images are saved in 8-bit format and can be viewed using NIH ImageJ® software.

3. Results

3.1. Instrument characterization

We measured the lateral resolution of the handheld instrument by performing en-face (XY-plane) imaging of a standard (USAF 1951) resolution target mounted on an additional Y-axis scanner (P601.4SL, 0–400 μm , Physik Instrumente, Auburn, MA) that is placed outside of the instrument. The 1-D MEMS scanner inside the instrument performed X-axis scanning. The axial resolution was determined by measuring the full width at half-maximum (FWHM) of the signal reflected from the surface of a chrome coated mirror through a scattering-free deionized-water film between the mirror and the SIL to simulate the optical thickness of the tissue. The lateral resolution from the en-face reflectance image is ~ 4 μm (group 7, element 5), Fig. 4(a). The measured axial resolution was ~ 5 μm with 671 nm illumination, Fig. 4(b).

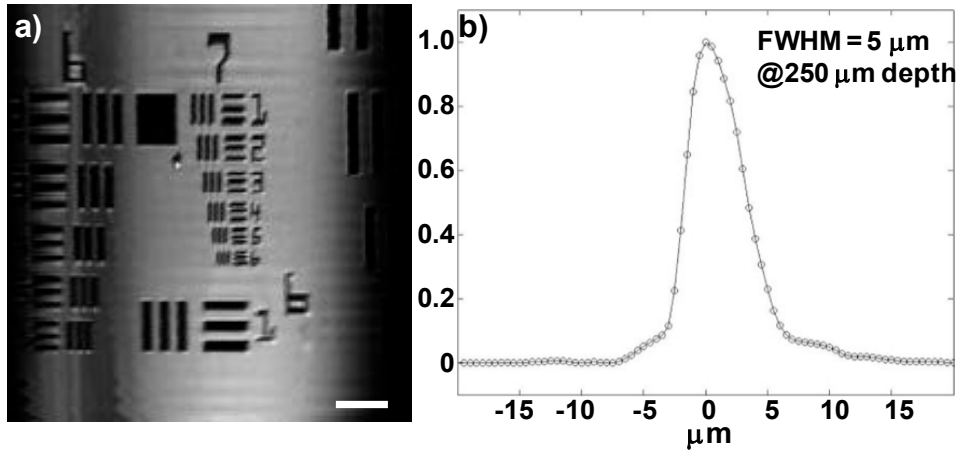


Fig. 4. Instrument resolution. (a) En-face (XY-plane) reflectance image of a standard target shows lateral resolution of 4 μm , FOV $400 \times 400 \mu\text{m}^2$, scale bar 50 μm . (b) Axial scan from a reflective target shows FWHM of 5 μm at depth of 250 μm in a scattering-free deionized-water film.

3.2. NIR vertical cross-sectional fluorescence (XZ-plane) imaging of colonic dysplasia *ex vivo*

We demonstrate vertical cross-sectional images of NIR fluorescence in a mouse model of colonic dysplasia *ex vivo*. The chemical structure of the Cy5.5-labeled peptide specific for colonic dysplasia is shown, Fig. 5(a). The amino acid sequence LTTHYKL is connected by a GGGSK linker on the C-terminus to the Cy5.5 fluorophore to prevent steric hindrance. This targeting peptide was selected using *in vivo* phage display technology [17]. We use CPC;Apc mice that are genetically engineered to spontaneously develop pre-malignant colonic lesions similar to that seen in human disease. Mice were cared for with approval of the University Committee on the Use and Care of Animals (UCUCA) at the University of Michigan and housed in specific pathogen-free conditions and supplied water *ad libitum*. CPC;Apc mice of age 6–7 months were injected with the Cy5.5-labeled peptide, LTTHYKL-GGGSK-Cy5.5, hereafter LTT*-Cy5.5, at a concentration of 400 μM via tail vein. LTT*-Cy5.5 was allowed to circulate for 15 minutes. The mice were then euthanized, and the colon was excised, washed, blotted dry, and mounted on glass slides using 3M Vetbond tissue adhesive. The fresh colonic mucosa were imaged immediately with 2 mW of excitation at $\lambda_{\text{ex}} = 671 \text{ nm}$. The tissues were then fixed with 10% buffered formalin for 24 hours, paraffin-embedded and sectioned into 10 μm thin slices and stained with hematoxylin and eosin (H&E). Histology was captured on an Axioskop2 upright microscope (Carl Zeiss Microimaging, Inc. Thornwood, NY).

NIR fluorescence images of colon show dysplastic crypts in the vertical orientation, Fig. 5(b), demonstrating the histology-like performance over a FOV of 800 μm (width) \times 400 μm (depth). The contrast from specific binding of the LTT-Cy5.5 peptide can be appreciated by the image of the border between normal colonic mucosa and dysplasia, Fig. 5(c). The arc seen at the top of this image is likely produced by the interface between the SIL and tissue that results from post-objective scanning. Vertically oriented crypts can be appreciated in the corresponding histology (H&E), scale bar 200 μm , Fig. 5(d). Use of a specific binding peptide allows for the transition from normal to pre-malignant mucosa to be visualized with high contrast using the same gain on the PMT. Compared to normal colonic mucosa, the NIR fluorescence intensity of dysplasia is >3 . The peptide binds to cells in the epithelium (~ 150 to 200 μm), and tissue below is not expected to produce signal. A control for this peptide has been demonstrated previously [17].

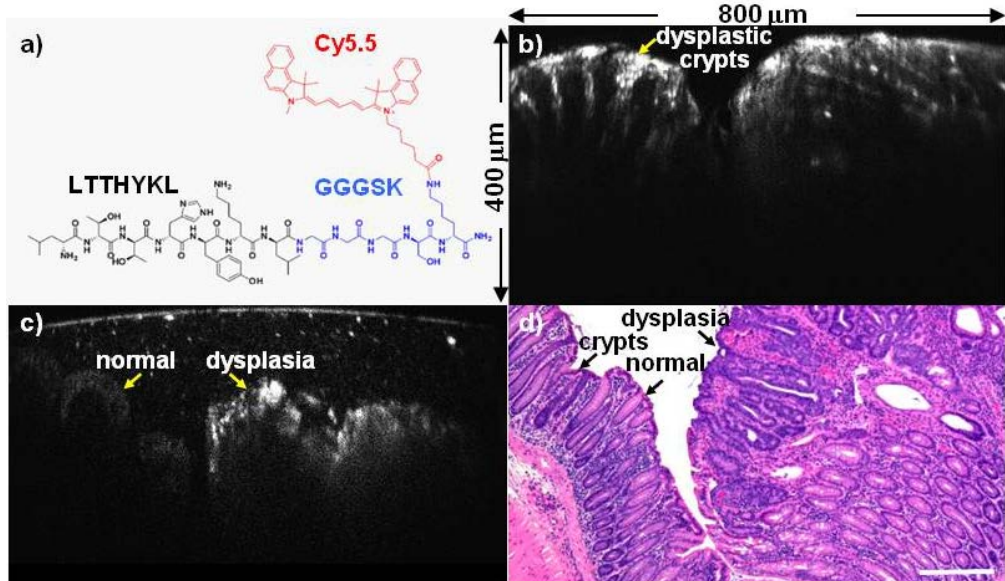


Fig. 5. Vertical cross-sectional image of colonic dysplasia. (a) Chemical structure of LTTHYKL peptide (black) with GGGSK linker (blue) and Cy5.5 fluorophore (red). (b) NIR fluorescence image from CPC;Apc mouse colon ex vivo shows vertically oriented dysplastic crypts. ($800 \times 400 \mu\text{m}^2$ FOV) (c) The border between normal colonic mucosa and dysplasia shows increased contrast from specific binding of the LTT*-Cy5.5 peptide. ($800 \times 400 \mu\text{m}^2$ FOV) (d) Corresponding histology (H&E), scale bar 200 μm .

4. Discussion

Here, we present a novel NIR dual axes confocal fluorescence endomicroscope that performs vertical cross-sectional (XZ-plane) imaging with an $800 \times 400 \mu\text{m}^2$ FOV up to 10 Hz in a handheld package. This FOV represents a significant improvement over that of other endomicroscope designs. This performance is achieved with use of the compact low-inertia XZ-plane scanner. In this instrument, a MEMS resonant scanner can produce large mechanical scan angles up to ± 7 degrees (peak amplitude) at low drive voltages (<40V). This resonant scanner is very stable and relatively insensitive to mechanical vibrations in the orthogonal direction. Thus, the fast X-axis tilting motion can be decoupled from the Z-axis displacement, which allows us to implement the XZ scanner directly with a high frame rate in a raster scanning pattern. Also, we can realize the desired scanning angle by tuning the pulse width modulation (PWM), drive voltage, or drive frequency in accordance to the MEMS scanner's frequency response, Fig. 2(b).

We also demonstrated the use of a NIR-labeled peptide to target and distinguish pre-malignant colonic mucosa from normal on vertical cross-sectional imaging in the CPC;Apc mouse ex vivo. This view provides a comprehensive picture of the differentiation pattern of the epithelium and is the standard used by pathologists to diagnose disease. The use of peptides may be sensitive to molecular changes that develop well in advance of morphological alterations to allow for disease detection at an earlier stage. Moreover, the use of bright fluorophores in the the dual axes design is important to overcome the low collection NA. This instrument can currently be used clinically for in vivo endomicroscopy in the rectum, and can be applied to the remainder of the colon when scaled down in size.

By comparison, the previous use of staggered vertical comb-drive actuators resulted in a XY-plane FOV of $362 \times 212 \mu\text{m}^2$ with high drive voltages [14]. Moreover, the Z-axis movement used an open-loop offset sliding mechanism [14], which is driven by a slow (<0.5 Hz) miniature electromagnetic motor that induces parasitic motions and deteriorates the Z-axis performance over time. In other endomicroscope designs, en-face (XY-plane) imaging is

performed by stacking images along the Z-axis in sequence. Vertical cross-sectional images are then reconstructed from post-processed 3-D volumetric images. This approach can be susceptible to motion artifacts and may be limited for in vivo imaging applications. In the future, we will scale down the size of this instrument to an OD 5mm package using a novel thin-film PZT technology [20] for real time in vivo imaging in small animals and in the clinic.

5. Conclusions

We demonstrate use of a novel, handheld endomicroscope based on the dual axes confocal architecture to collect NIR fluorescence images in vertical cross-sections over a large FOV ($800 \times 400 \mu\text{m}^2$) to detect Cy5.5-labeled peptides that bind specifically to pre-malignant colonic mucosa. This instrument can potentially be used in vivo to guide tissue biopsy and stage disease progression when scaled down further in size.

Acknowledgments

The authors acknowledge support from the University of Michigan Rackham International Student Fellowship (Z. Q.) and from NIH R01 CA142750 and U54 CA136429 (T. D. W.). We thank H. Schenk for discussion on the MEMS resonant scanner, A. Shih for advice on the precision instrument development, T. Donajkowski for discussion and support of miniature endomicroscope prototyping, and J. Y. Cho for support with laser cutting in K. Najafi's MEMS research lab.